Available online at www.sciencedirect.com
ScienceDirect
Journal of Solid State Chemistry 180 (2007) 2290–2297
JOURNAL OF SOLID STATE CHEMISTRY
www.elsevier.com/locate/jssc

Sol–gel synthesis of hydrous ruthenium oxide nanonetworks from 1,2-epoxides

Jeremy Walker[a], R. Bruce King[b], Rina Tannenbaum[a,*]

[a]School of Materials Science and Engineering, Georgia Institute of Technology, Atlanta, GA 30332, USA
[b]Department of Chemistry, University of Georgia, Athens, GA 30602, USA

Received 22 February 2007; received in revised form 29 May 2007; accepted 31 May 2007
Available online 6 June 2007

Abstract

Hydrous ruthenium oxide ($RuO_2 \cdot xH_2O$) xerogels were synthesized through the addition of a 1,2-epoxide, propylene oxide, to commercial hydrated ruthenium chloride, "$RuCl_3 \cdot xH_2O$," in ethanol. After a blue-black monolithic gel formed in 4 h, the samples were allowed to age for 24 h and were dried in ambient conditions. The dried samples were then characterized by XPS, XRD, DTA and TGA. XPS showed the Ru($3d_{5/2}$) peak at a binding energy of 281.7 eV, corresponding to that of hydrous ruthenium oxide. XRD data revealed the synthesized material as amorphous. Heating the sample in inert atmospheres caused the complete reduction of the oxide to the zero-valent state, whereas heating the sample in air resulted in both crystalline anhydrous RuO_2 and zero-valent ruthenium, depending on the method of heating. DTA traces showed an endotherm ending at 150 °C, corresponding to the loss of coordinated water, as well as two higher temperature crystallization exotherms when the sample was heated in both inert and oxygen-rich atmospheres. TGA runs also confirmed the complete reduction of the hydrous oxide when heated in nitrogen below 270 °C and the formation of anhydrous ruthenium oxide when heated in air, confirming the XRD results.

Keywords: Sol–gel chemistry; Hydrous ruthenium oxides; Ruthenium oxide nanonetworks

1. Introduction

Anhydrous ruthenium oxide materials possess versatile functionalities and properties that make them useful in numerous industries. RuO_2 is known as an exceptional electrode material for high-power and high-energy density capacitors as a result of its high capacitance [1] and exhibits low resistivity and good thermal stability [2,3]. It is also known to be a metallic conductor [4–6] and has been used as a catalyst for organic and inorganic reactions [7,8], an anode material in the production of chlorine [9], and in cryogenic temperature sensors [10]. RuO_2 is also a good candidate for the bottom electrode for high dielectric constant capacitors owing to its etching capability [11]. Hydrous ruthenium oxide, $RuO_2 \cdot xH_2O$, can be used as an electrochemical capacitor due to its high-energy density [12]. These hydrous materials possess high capacitance, low resistance [13], and good electrochemical cyclability [14] with maximum capacitance values of the material occurring when $x \sim 0.5$ [15].

Ruthenium oxides have been prepared by sputtering [16], cathodic electrosynthesis [17], and solution chemistry including thermal decomposition of hydrated $RuCl_3$ [18] and sol–gel processes [19,20]. Suh et al. [13] have demonstrated that the sol–gel epoxide addition method can produce ruthenium oxide aerogels of high porosity from hydrated ruthenium chloride solutions. The sol–gel process is a very versatile synthesis method for the formation of a porous oxide with controlled dimensions of the particle sizes. Previous work involving iron(III) oxides from hydrated iron salt precursors in the presence of epoxides [21–25] has demonstrated that the sol–gel process can generate a network material having particles with nanoscale features, high porosity, high surface area, and low density [22,23]. This epoxide addition in the sol–gel formation of metal oxides has also been successful in the synthesis of other technologically relevant oxides such as

*Corresponding author. Fax: +1 404 894 9140.
E-mail address: rinatan@mse.gatech.edu (R. Tannenbaum).

0022-4596/$ - see front matter © 2007 Elsevier Inc. All rights reserved.
doi:10.1016/j.jssc.2007.05.031

NiO [26], Al_2O_3 [27], Cr_2O_3, ZrO_2, WO_3, as well as numerous other transition metals [28].

Our particular interest in exploiting these properties lies in the design of metal oxide matrices for energetic materials. Such energetic materials are comprised of a particulate metal fuel (e.g., Al, Fe, Cr) closely mixed with metal oxide particles, which, after a stress-induced oxidation–reduction reaction, result in a substantial exothermic heat release. In these materials, reactions between different metal oxide networks (oxidants) and dispersed metallic particles (fuels) will result in different energetic release rates. The efficiency of the exothermic output of the energetic reaction is also governed by the interfacial area and reactivity between the metal fuel and the metal oxide particles and hence, reducing the size of the metal oxide (oxidant) network as well as the size of the particulate metal fuel to the nanometer scale, will dramatically increase the interfacial area and will directly translate into a higher efficiency of the oxidation–reduction reaction.

In this work, we extend the sol–gel synthesis of hydrous ruthenium oxide involving the addition of an epoxide, e.g., propylene oxide, to a hydrated ruthenium chloride precursor solution, to generate a porous ruthenium oxide xerogel with nanoscale dimensions of the oxide particles. Unlike the work of Suh et al. [13] that is specifically focusing on the formation of highly porous ruthenium oxide aerogels by carbon dioxide supercritical drying, our interest lies mainly in the formation and thermal behavior of the denser xerogel material. In view of the potential application of such oxides as energetic materials, the main factor of interest in our case is the possibility of formation of tight reactive interfaces between the ruthenium oxide "nanonetwork" and the fuel nanoparticles, and the influence of the increase in the local temperature on the chemistry of the reactants. Despite the fact that the electronic configuration of Ru is similar to that of Fe, the chemistry of its oxides bears little resemblance to that of iron. While there is extensive chemistry associated with the M_xO_y (M = Fe or Ru) species for both elements, the higher oxidation states of Ru are much more easily obtained than for iron. Hence, in this paper, we set out to probe the synthesis, thermal stability, and reactivity of hydrous ruthenium oxide nanonetworks as the potential oxidation moiety in energetic materials systems.

2. Experimental

2.1. Synthesis of hydrous ruthenium oxide gels

Ruthenium-(III) chloride hydrate, $RuCl_3 \cdot xH_2O$; and propylene oxide, C_3H_6O, were purchased from Fisher Scientific and used as received. Stock absolute ethanol was obtained from Aldrich and used as received. The synthesis was performed in a 20 mL glass scintillation vial under ambient conditions by adding 0.42 g (1.6 mmol) $RuCl_3 \cdot xH_2O$ to 3.5 mL of ethanol and stirring until the powdered ruthenium chloride component was completely dissolved in the ethanol. (The estimate of 1.6 mmol of Ru was calculated by using the exact formula of the Ru precursor, $RuCl_{3.37} \cdot 2.5H_2O$, having a molecular weight of 265.6 g/mol, which was obtained after performing elemental analysis on the as-bought $RuCl_3 \cdot xH_2O$ salt. However, the commercially available hydrated ruthenium-(III) chloride is a mixture of several phases, including the hydrate of ruthenium-(IV) oxide derivatives [29].) Then a 1.2 mL allotment of the weak base, propylene oxide, was added as the gelation chemical to the solution and stirred. The time to gelation was monitored and recorded after the addition of the gelation chemical. After gelation occurred, the gel was covered and allowed to age for 24 h. Then the aged gel was allowed to dry in a fume hood under ambient conditions to allow solvents to evaporate. To complete solvent evaporation, the sample was placed under vacuum for an additional 48 h.

2.2. Physical characterization of synthesized material

The dried xerogel material was ground into a fine powder using a ceramic mortar and pestle. XPS scans of powder samples were taken using a Surface Science Laboratories SSX-100 ESCA Spectrometer using monochromatic Al$K\alpha$ radiation (1486.6 eV). The system operated at a pass energy of 50 eV. Powder samples were housed in aluminum foil during analysis and a flood gun was used at a voltage of 3 eV. The operating pressure of the vacuum chamber was less than 3×10^{-8} Torr. General scans covered the binding energy range of 0–1100 eV. Thirty high-resolution C($1s$)/Ru($3d_{5/2}$) scans were run with a central binding energy (CBE) of 285 eV with a window width of 20 eV at a spot size of 400 μm. Also, 30 high-resolution O($1s$) scans were run at a CBE of 532 eV using a spot size of 400 μm and a window width of 20 eV. Each high-resolution scan possessed a 0.1 eV per step interval. Curve fitting of the data was accomplished using the program Spectral Data Processor, Version 4.1.

XRD of the samples was performed on a Philips PW 1800 X-ray diffractometer. Patterns from 20° to 85° were examined with a step size of 0.02° using monochromatic Cu$K\alpha$ X-rays with a wavelength of 1.54056 Å. Powder samples were analyzed using a zero background sample holder.

HRTEM images were obtained from a Hitachi HF 2000 FE TEM operating at an accelerating voltage of 200.0 keV. Elemental analysis of the material was performed by Atlantic Microlabs, Norcross, GA. Quantitative values of carbon, hydrogen, oxygen, and chlorine were determined through experimental measures. The balance of the compositional make-up of the sample was assigned as ruthenium. Lower temperature DSC data were compiled from a TA Instruments Q100 DSC up to temperatures of 550 °C. Samples were placed in aluminum pans and heated at 10 °C/min with a nitrogen purge at 20.00 mL/min. High-temperature DTA/TGA data (>600 °C) was determined using a Netzsch STA 449-Jupiter TGA-DSC. Powder

samples were placed in alumina crucibles and heated at 10 °C/min in both air and argon atmospheres.

As a cautionary note, to the best of our knowledge, the chemical, physical and toxicological properties of ruthenium oxide have not been thoroughly investigated and recorded. What is certain is the fact that it is irritating to skin and mucous membranes. The oxidation of ruthenium and/or ruthenium compounds may form the volatile, toxic and highly irritating ruthenium-(VIII) oxide, and hence all reactions are performed in a well-vented hood and according to appropriately recommended safety procedures.

3. Results and discussion

3.1. Synthesis and characterization of hydrous ruthenium oxide gels

The addition of propylene oxide to a commercial hydrated ruthenium chloride precursor solution (assumed to contain mainly Ru(IV) as "$Ru(OH)Cl_3$") results in a heat-releasing reaction with the formation of a blue-black monolithic wet gel in 4 h, as compared to 25 min for the formation of an iron oxide gel from the $FeCl_3 \cdot 6H_2O$ precursor hydrous salt. The slower kinetics in the formation of the ruthenium oxide nanonetwork as compared to those of iron oxide nanonetworks may result from a greater kinetic inertness of Ru(III) and Ru(IV) relative to Fe(III) [29]. A porous xerogel of hydrous ruthenium oxide ($RuO_2 \cdot xH_2O$) forms after residual solvents in the gel are allowed to evaporate in ambient conditions. Fig. 1 shows a HRTEM image of the synthesized material, which reveals a porous microstructure having clusters with diameters ranging from 40 to 80 nm.

X-ray photoelectron spectroscopy was utilized to evaluate the composition of the ruthenium oxide material, $RuO_2 \cdot xH_2O$, synthesized from the weak base propylene oxide. Fig. 2(a) shows the general survey spectrum of the material. Further analysis of the XPS spectrum was performed by high-resolution scans of the C(1*s*)/Ru(3*d*) and O(1*s*) regions. Fig. 2(b) shows the high-resolution C(1*s*)/Ru(3*d*) region having adjusted the C(1*s*) peak to 285.0 eV to compensate for the presence of charging effects in the material [30]. This region can be deconvoluted into five separate peaks, three related to the C(1*s*) photoelectrons and two associated with the Ru($3d_{5/2}$) and Ru($3d_{3/2}$) peaks: (A) at a binding energy (BE) of 281.7 eV corresponding to the Ru($3d_{5/2}$) peak of the material, (B) at a BE of 285.0 eV corresponding to aliphatic C–C bonding arising from residual ethanol as well as the chloropropanol and propanediol intermediates resulting from the sol–gel formation process [21], (C) at a BE of 286.3 eV corresponding to the Ru($3d_{3/2}$) peak of the material, (D) the more electronegative C–Cl species at a binding energy of 287.5 eV originating from the chloropropanol species, and (E) at a BE of 288.7 corresponding to the C–O bonding from the same organic compounds mentioned in (A). (E) is located at the highest BE owing to the highest electronegativity of oxygen. It is important to note the absence of an epoxide peak in the C(1*s*)/Ru(3*d*) high-resolution scan. This is due to the fact that propylene oxide is a key component in the reaction and, unlike a traditional catalyst, it actually gets consumed during the reaction [21]. The Ru($3d_{5/2}$) peak of the material is located at a binding energy of 281.7 eV whereas the related Ru($3d_{5/2}$) binding energy peak of elemental ruthenium is at 280.0 eV [7]. It is known that non-equivalent atoms of the same element in a solid give rise to peaks with different BE with increasing BE for increasing oxidation state [31]. The Ru($3d_{5/2}$) peak of the material is located at a higher BE than the same peak for anhydrous RuO_2, i.e., 280.7–281.0 eV [32], owing to the presence of –OH functional groups on Ru [33]. In this context, it has been reported that the Ru($3d_{5/2}$) peak for a hydrous ruthenium oxide is located at a BE of 281.4–281.8 eV [34]. Therefore, based on the analysis of the deconvolution of the Ru($3d_{5/2}$) region, it is possible to identify the synthesized material as a hydrous ruthenium oxide, $RuO_2 \cdot xH_2O$.

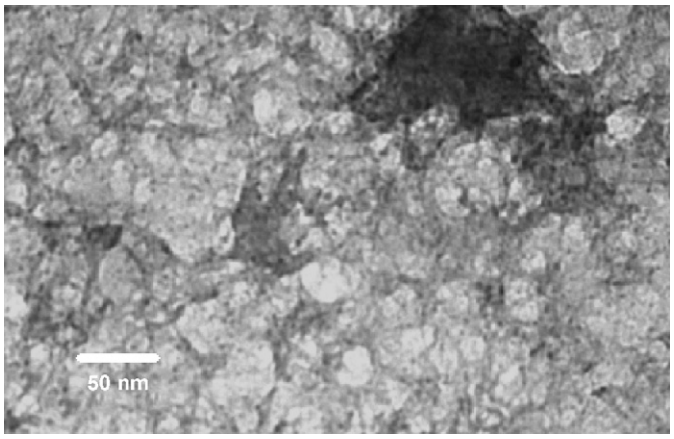

Fig. 1. High-resolution transmission electron microscopy (HRTEM) image of the as-synthesized hydrous ruthenium oxide gel, exhibiting the presence of clusters on the order of 40–80 nm.

The O(1*s*) region can be deconvoluted into three peaks: (F) 529.5 eV corresponding to the lattice oxygen within the ruthenium oxide; (G) 530.8 eV corresponding to the oxygen within the chemisorbed water in $RuO_2 \cdot xH_2O$ [35]; and (H) 532.5 eV corresponding to the oxygen–carbon bonding of the residual organic diol species from the synthesis as well as residual ethanol. The relative ratios between the three experimental O(1*s*) peaks corresponding to RuO_2, $RuO_2 \cdot xH_2O$, and O–C are 31.1:50.6:18.3, respectively. This indicates that the majority of the synthesized product (~81.7%) is a hydrated ruthenium oxide, with the balance of the sample oxygen originating from residual organic species. The reported O(1*s*) peak location for a hydrated ruthenium oxide is 529.3 eV for the oxide and 530.5 for the oxygen within the adsorbed H_2O [7]. These O(1*s*) values are comparable to the values reported in the synthesized material here. Whereas the O(1*s*) peak of elemental oxygen is centered at 532.0 eV, the BE of the oxygen peak of an

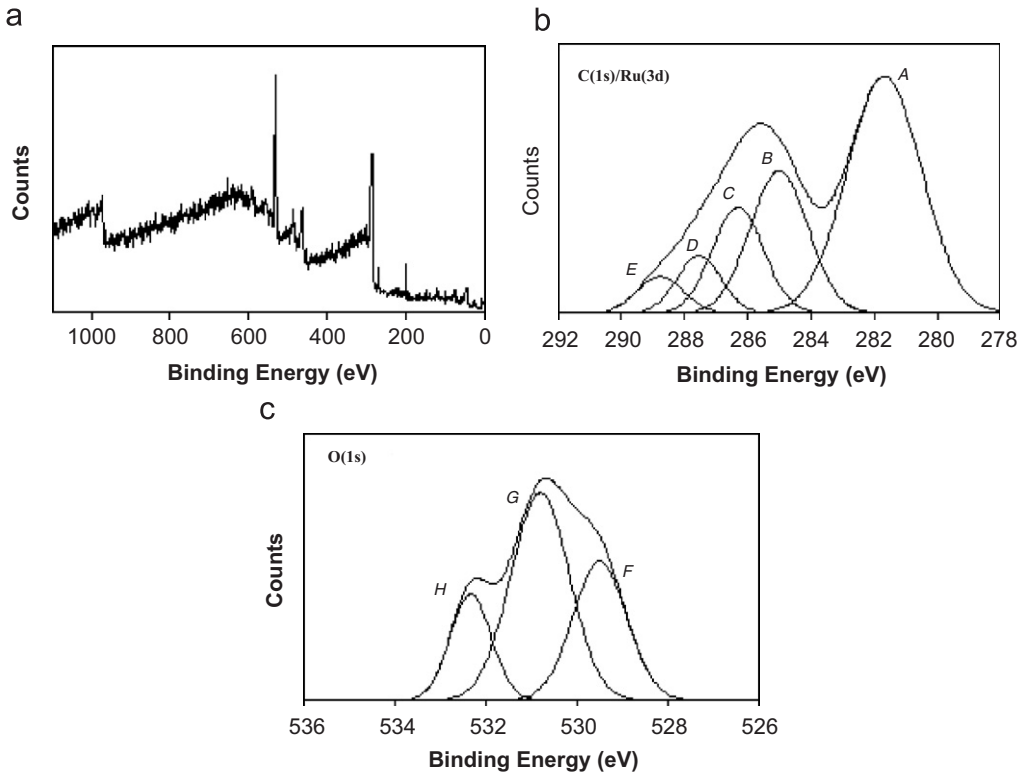

Fig. 2. The X-ray photoelectron spectra (XPS) of a sol–gel synthesized hydrated ruthenium oxide from the weak base propylene oxide. (a) The general scan of the oxide material. (b) The high-resolution C(1*s*)/Ru(3*d*) core level electrons and its deconvolution into five peaks. (c) The O(1*s*) core level emission spectrum and its deconvolution into three peaks.

oxide is lower than pure oxygen–again proving the existence of a ruthenium oxide material [36]. The O(1*s*) region is shown in Fig. 2(c). Also observed in the general scan of the material is the existence of the Cl(2*s*) and Cl(2*p*) peaks originating from the chloride species of the initial precursor and the chloropropanol species at BE of 269.7 and 199.3 eV, respectively, and the Al($2s_{1/2}$), Al($2p_{1/2}$) and Al($2p_{3/2}$) peaks originating from the Al foil used to house the powder sample in the XPS instrument. The XPS data for the as-synthesized material are summarized in Table 1.

3.2. Temperature-dependent formation of ruthenium oxide species

Figs. 3 and 4 show X-ray diffraction data for the as-synthesized sample as well as patterns for the sample after various heat treatments. Figs. 3(a) and (b) display the diffraction pattern of the as-prepared gel and the gel heated to 125 °C for 2 h under nitrogen, respectively. These patterns show that the synthesized material is amorphous with crystallization not occurring until temperatures greater than 125 °C. Fig. 3(c) shows the diffraction pattern of a gel specimen heated to 250 °C and held for 2 h under nitrogen. The onset of low levels of crystallinity may be observed at this temperature, generating broad peaks in the vicinity of Bragg angles of 38°, 44°, and 70°. Fig. 3(d) shows the XRD pattern of a sample heated to 550 °C at 10 °C/min under nitrogen using a DSC. At this temperature, the material exhibits a higher degree of crystallinity with peaks at 38.43°, 42.21°, 44.11°, 58.52°, 69.48°, 78.53°, and 84.75°. The broad peaks in Figs. 3(c) and (d) are indicative of the presence of zero-valent ruthenium metal, while the peaks listed in Fig. 3(d) correspond directly and unequivocally to the (1 0 0), (0 0 2), (1 0 1), (1 0 2), (1 1 0), (1 0 3), (1 1 2), and (2 0 1) planes of $Ru^{(0)}$, respectively. Fig. 3(e) shows the continued trend of the complete reduction process of the hydrated ruthenium oxide

Table 1
The binding energies, full-width half-maximum values, percentage of total peak area, and assignment of atoms of the X-ray photoemission spectrum (XPS) of the O(1*s*) and C(1*s*)/Ru(3*d*) core electron regions for a hydrous ruthenium oxide sample synthesized by the sol–gel process from propylene oxide, corresponding to Fig. 2

Peak label	BE (eV)	FWHM (eV)	% of total area	Assignment of atoms
C(1*s*)/Ru(3*d*)				
A	281.7	2.77	49.7	Ru($3d_{5/2}$)
B	285.0	2.15	23.1	C–C
C	286.3	1.91	15.2	Ru($3d_{3/2}$)
D	287.5	1.64	7.2	C–Cl
E	288.7	1.71	4.7	C–O
O(1*s*)				
F	529.5	1.39	31.1	RuO_2
G	530.8	1.51	50.6	$RuO_2 \cdot xH_2O$
H	532.5	1.06	18.3	O–C

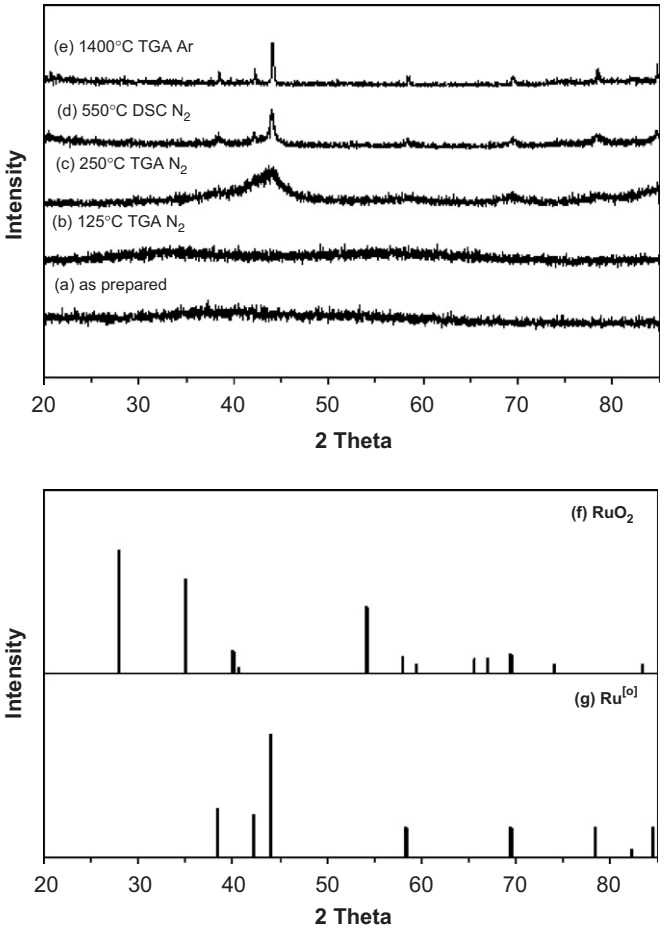

Fig. 3. X-ray diffraction (XRD) patterns of the sol–gel synthesized hydrous ruthenium oxide samples heated in inert atmospheres to (a) room temperature, (b) 125 °C, (c) 250 °C, (d) 550 °C, and (e) 1400 °C and published diffraction patterns for (f) anhydrous RuO_2 and (g) $Ru^{(0)}$.

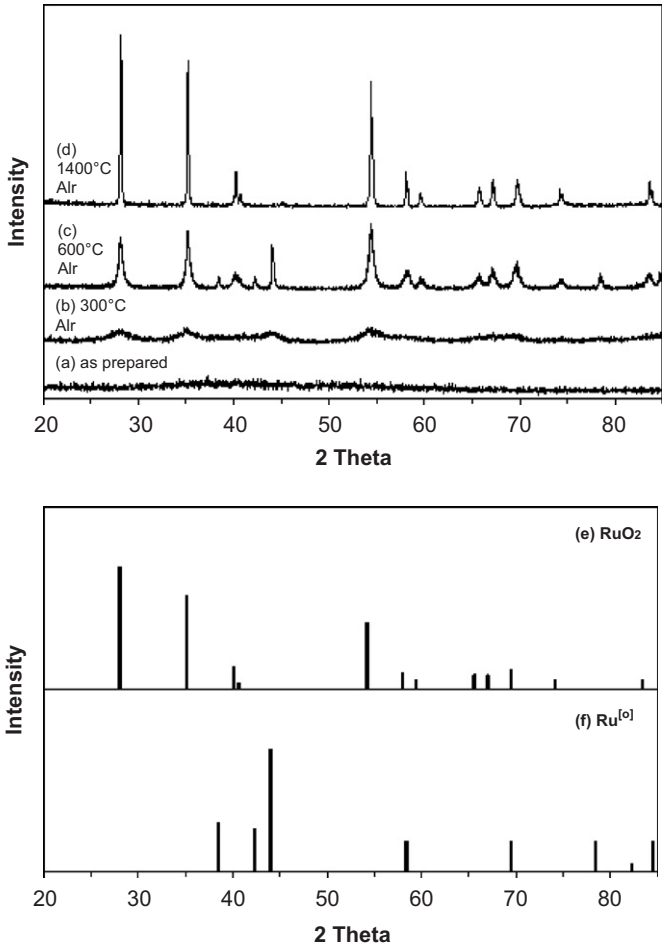

Fig. 4. X-ray diffraction (XRD) patterns of the sol–gel synthesized hydrous ruthenium oxide samples heated in air at (a) room temperature, (b) 300 °C, (c) 600 °C, and (d) 1400 °C and published diffraction patterns for (e) anhydrous RuO_2 and (f) $Ru^{(0)}$.

material to ruthenium metal in an inert atmosphere when heated to 1400 °C. Figs. 3(f) and (g) show the diffraction patterns for $Ru^{(0)}$ and RuO_2. Ji et al. [34] have stated that the reduction of hydrous ruthenium oxide to ruthenium metal is due to the presence and affinity of chloride ions, which are generated from the ruthenium chloride precursor salt involved in the sol–gel reaction, to act as intramolecular reducing agents, as shown by

$$Ru^{IV}O_2 + 4Cl^{1-} \xrightarrow{\Delta,\ \text{Inert Gas}} Ru^{(0)} + 2Cl_2 + 2O^{2-}. \quad (1)$$

Pagnaer et al. [37] have postulated also the possibility that the organic matrix, stemming from the organic solvent and gelation agent, is oxidized during heating, forming carbon monoxide, which is another potential reducing agent, as shown by

$$Ru^{IV}O_2 + 2CO \xrightarrow{\Delta,\ \text{Inert Gas}} Ru^{(0)} + 2CO_2. \quad (2)$$

The reduction of the ruthenium oxide that ensues at temperatures below 250 °C is most likely due to the thermodynamically driven propensity of ruthenium oxide to decompose to the zero-valent state under low oxygen partial pressure, as is the case within the instrument housings of the TGA and DSC under inert gas purging. Hence, a possible reaction sequence that could account for the products observed in this sol–gel reaction is as follows:

$$4Ru^{III}Cl_3 \xrightarrow[\text{Air}]{\text{EtOH, Propylene oxide}} Ru^{(0)} + 3Ru^{IV}O_2, \quad (3)$$

$$Ru^{IV}O_2 \xrightarrow{\Delta,\ \text{Inert Gas}} Ru^{(0)} + O_2. \quad (4)$$

As shown in Eq. (3), Ru^{III} undergoes disproportionation to $Ru^{(0)}$ and Ru^{IV}. The absence of oxygen, or the low oxygen partial pressure during heating cycles under inert atmosphere, destabilizes the ruthenium oxide compound and drives the reduction reaction shown in Eq. (4). The presence of $Ru^{(0)}$ immediately upon the completion of the sol–gel reaction, as indicated by Eq. (3), cannot be confirmed because of three main reasons: (1) the ambiguity in the assignment of the XPS peaks, owing to the overlap

of the Ru($3d_{5/2}$) and Ru($3d_{3/2}$) regions with those of C(1*s*), (2) the very large FWHM of the 281.7 eV band assigned to Ru($3d_{5/2}$), which could also be deconvoluted into an additional band in the vicinity of 280.0 eV corresponding to $Ru^{(0)}$, and (3) the amorphous character of the product that does not afford any conclusion based on the X-ray diffraction below 125 °C.

Indirect evidence of the initial formation of $Ru^{(0)}$ from the sol–gel reaction may be obtained when examining the behavior of the product mixture upon heating in air. Whereas heating the sample in an inert environment results in the complete reduction of the hydrated ruthenium oxide to the zero-valent state, heating the sample in air results in the formation of an anhydrous ruthenium oxide material. However, the presence of zero-valent Ru upon heating is still observed under certain conditions. Fig. 4(a) shows the XRD pattern of the as-prepared amorphous material and Fig. 4(b) shows the sample heated to 300 °C for 20 h in air, where the peaks corresponding to anhydrous ruthenium oxide begin to emerge. Broad peaks can be seen at Bragg angles of 28.4°, 35.3°, 44.2°, 54.4°, and 69.7°. The first three of these peaks match the most intense peaks of anhydrous RuO_2 corresponding to the (1 1 0), (1 0 1), and (2 1 1) planes. Fig. 4(c) shows an XRD pattern of the material heated at 600 °C for 20 h in air showing a more crystalline RuO_2. However, peaks related to zero-valent ruthenium clearly remain in these patterns. Fig. 4(d) displays the XRD pattern of the sample heated at 10 °C/min under air to a temperature of 1400 °C. It is not until this temperature that the complete oxidation of all ruthenium within the sample occurs resulting in a pure anhydrous ruthenium oxide, shown by

$$Ru^{(0)} \xrightarrow{1400\,^{\circ}C,\ O_2} Ru^{IV}O_2. \quad (5)$$

Another possible explanation for the presence of $Ru^{(0)}$ in the samples is that some of the surface oxygen atoms in the samples heated in air to 300 and 600 °C, generated by the thermodynamic instability of the ruthenium oxide with increased temperature, may have desorbed owing to the lack of a sufficient supply of atmospheric oxygen to replenish the lost oxygen. This decomposition results in a $Ru^{(0)}$ surface and bulk anhydrous RuO_2, consistent with the presence of both phases in the XRD patterns. However, heating the sample to 1400 °C in the TGA can replenish the surface oxygen liberated from this high-temperature thermal decomposition due to a continuous source of oxygen flowing over the sample surface. This maintains a high oxygen partial pressure and prevents this spontaneous decomposition, thereby resulting in a single-phase material, anhydrous RuO_2, as seen in the XRD pattern.

This change in material composition after heating the sample to different temperatures under different atmospheres can be further evaluated from thermo-gravimetric analysis (TGA) profiles. Fig. 5 shows the changes in the mass fraction of the two samples upon heating under two

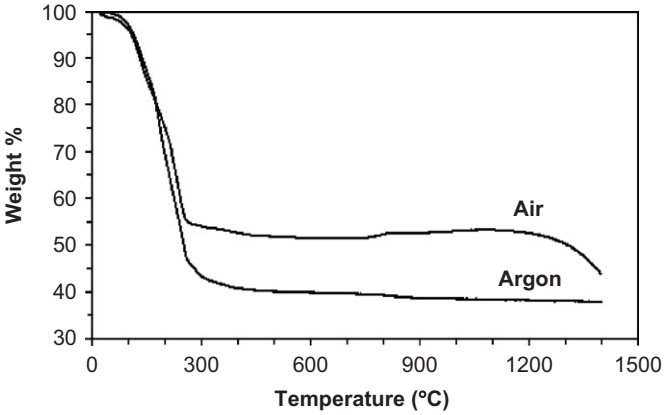

Fig. 5. Thermogravimetric analysis (TGA) thermal profile for the decomposition of hydrated ruthenium oxide samples heated to 1400 °C at a heating rate of 10 °C/min in two different atmospheres, air and argon. Note an almost zero-weight loss for the sample heated in argon above 300 °C, whereas the sample heated in air retains a larger mass percentage above this temperature until high-temperature ruthenium oxide thermal decomposition causes mass loss above 1000 °C.

different atmospheres, namely air and argon. Both samples lose a substantial fraction of their mass up to ~270 °C. The sample heated in air loses ~45% and the sample heated in argon loses ~55% of their respective total weights. This loss is attributed to loss of adsorbed water in the material as well as the loss of residual organics remaining from the initial ambient drying procedure. For the sample heated in an inert atmosphere, weight loss essentially ceases at this temperature until 1400 °C. The TGA results also confirm that the as-prepared hydrous ruthenium oxide is reduced to the zero-valent state when heated in an inert atmosphere, in accord with the XPS and XRD data. If the weight loss data in both atmospheres, air and argon, is normalized between the temperatures 300 and 1000 °C (the temperature range where almost no weight loss is observed), a simple weight ratio of Ru metal to RuO_2 (0.76) is equal to the normalized ratio of the weights of the samples heated in argon and air (0.77). This value shows that the sample heated in argon does not have the associated weight of the two oxygens in RuO_2 and the additional 10% weight loss below 300 °C can be considered a result of the liberation of oxygen formerly coordinated with the oxide. Also, at 1400 °C, the total remaining weight percent is 37.8%. This corresponds well to the total weight percent of 35.5% of ruthenium of the synthesized material found by elemental analysis. Therefore, the sample heated in argon can be considered $Ru^{(0)}$ and the sample heated in air RuO_2.

Above 300 °C, the weight loss of the sample heated in air is minimal up to 1000 °C, at which point a drastic drop in weight is seen. This weight loss can be explained as spontaneous decomposition of the oxide at a temperature greater than 600 °C as the ruthenium–oxygen bonds break, and the oxygen is liberated as O_2 [38]. This decomposition may also explain the existence of $Ru^{(0)}$ in the XRD patterns of the samples heated in air, but not in the TGA, owing to insufficient flow of oxygen that could drive the

thermodynamic equilibrium completely towards the oxide, as shown by

$$RuO_2 \xrightarrow{T>600\,^{\circ}C} Ru(s) + O_2(g)\uparrow . \quad (6)$$

This high-temperature weight loss can also be explained by the reactions that occur when RuO_2 is heated in the presence of oxygen, as shown by [7]

$$RuO_2(s) + O_2(g) \xrightarrow{T\sim 800\,^{\circ}C} RuO_4(g)\uparrow ,$$

$$RuO_2(s) + \tfrac{1}{2}O_2(g) \xrightarrow{T>1000\,^{\circ}C} RuO_3(g)\uparrow . \quad (7)$$

In these reactions, higher valency gaseous ruthenium oxide species form on the surface of the sample and are eventually purged from the sample, resulting in a decrease in sample weight at high temperatures. $RuO_3(g)$ is the dominant species found at temperatures greater than 1000 °C and $RuO_4(g)$ is dominant around 800 °C [7]. As the sample heated in argon does not show a decrease in sample weight above 1000 °C, neither the ruthenium–oxygen bond decomposition nor the high-temperature formation of higher valency gaseous ruthenium oxide species occurs, indicating a complete absence of oxygen in the system and, therefore, the sole existence of $Ru^{(0)}$.

Fig. 6 shows the differential thermal analysis (DTA) data of the samples heated in air and argon from room temperature to 1400 °C. Both samples display small endotherms below 150 °C resulting from the loss of water [17]. The sample heated in air displays a sharp exotherm at 250 °C owing to crystallization of the as-synthesized amorphous material as well as a broad exotherm starting at 300 °C owing to a continued increase in crystallinity of the sample over the entire temperature range. The sample heated in argon displays a smaller exotherm at 235 °C owing to the competing endothermic decomposition of the hydrous oxide to $Ru^{(0)}$ with the exothermic crystallization of these zero-valent atoms in this temperature range. As with the sample heated in air, a broad exotherm beginning at 300 °C can be seen. Its magnitude is smaller owing to an overall lower level of crystallization. This relative increase in crystallinity for samples in both atmospheres is confirmed by the corresponding XRD patterns.

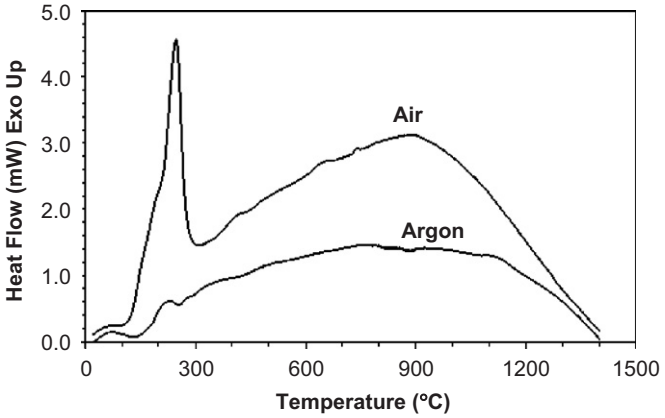

Fig. 6. Differential thermal analysis (DTA) data for the synthesized hydrous ruthenium oxide heated at 10 °C/min to 1400 °C in two different atmospheres, air and argon.

4. Conclusions

The objective of this work was to evaluate the use of a 1,2-epoxide in the sol–gel synthesis of hydrous ruthenium oxide from a ruthenium chloride solution. After verifying that gelation successfully occurs 4 h after the addition of the epoxide, characterization of the material was carried out by XPS, XRD, DTA, and TGA. Through deconvolution of the C(1*s*)/Ru(3*d*) region, XPS established that the synthesized gel material was a hydrous ruthenium oxide, $RuO_2 \cdot xH_2O$, which also contains residual organic species not removed during the drying process. After heating the hydrous ruthenium oxide in inert and oxygen-containing atmospheres to temperatures up to 1400 °C, evaluation of the XRD patterns showed that the as-prepared material was amorphous and samples heated in inert atmospheres were completely reduced to $Ru^{(0)}$ below 250 °C. XRD patterns of samples heated in air revealed the existence of anhydrous RuO_2 as well as $Ru^{(0)}$, unless a continuous supply of oxygen was present in the system, ensuring the presence of the high oxygen partial pressure required to maintain the oxide as the thermodynamically stable phase. DTA traces show an endothermic loss of water below 150 °C, with exotherms for samples heated in both air and argon owing to crystallization. The lower temperature exotherm of the sample heated in argon is smaller than that of the corresponding sample heated in air owing to the competing endothermic decomposition of the hydrous oxide into ruthenium metal and oxygen gas in the same temperature interval. TGA data also illustrate that the synthesized material contained approximately 45% organic material by weight. This organic material is evolved below 250 °C with the complete reduction of the original material to $Ru^{(0)}$ below 250 °C for the sample heated in argon. Also, TGA demonstrates that the sample heated in air becomes an anhydrous ruthenium oxide by this same temperature. Further, high-temperature weight loss is attributed to the well-known formation of gaseous higher valency ruthenium oxide species as well as high-temperature thermal decomposition of the RuO_2 species into ruthenium metal and oxygen gas.

Acknowledgments

This work was supported by the Air Force/Bolling AFB/DC MURI project on Energetic Structural Materials, award No. F49620-02-1-0382. The authors are indebted to Professors Thomas Sanders and Naresh Thadhani of Georgia Institute of Technology for their insightful and helpful comments.

References

[1] I.-H. Kim, K.-B. Kim, Electrochem. Solid-State Lett. 4 (2001) A62–A64.
[2] J.M.E. Harper, S.E. Hoernstroem, O. Thomas, A. Charai, L. Krusin-Elbaum, J. Vac. Sci. Technol. A 7 (1989) 875–880.
[3] L. Krusin-Elbaum, M. Wittmer, D.S. Yee, Appl. Phys. Lett. 50 (1987) 1879–1881.
[4] M.M. Jevtic, E.V. Jelenkovic, K.Y. Tong, G.K.H. Pang, Thin Solid Films 496 (2006) 214–220.
[5] D.A. McKeown, P.L. Hagans, L.P.L. Carette, A.E. Russell, K.E. Swider, D.R. Rolison, J. Phys. Chem. B 103 (1999) 4825–4832.
[6] K.E. Swider-Lyons, C.T. Love, D.R. Rolison, J. Electrochem. Soc. 152 (2005) C158–C162.
[7] K.S. Kim, N. Winograd, J. Catal. 35 (1974) 66–72.
[8] D.J. Suh, J. Non-Crystal. Solids 350 (2004) 314–319.
[9] A.J. Terezo, E.C. Pereira, Mater. Lett. 53 (4/5) (2002) 339–345.
[10] R. Sahul, V. Tasovski, T.S. Sudarshan, Sensors and Actuators A 125 (2006) 358–362.
[11] S. Bhaskar, P.S. Dobal, S.B. Majumder, R.S. Katiyar, J. Appl. Phys. 89 (2001) 2987–2992.
[12] W. Sugimoto, K. Yokoshima, K. Ohuchi, Y. Murakami, Y. Takasu, J. Electrochem. Soc. 153 (2006) A255–A260.
[13] D.J. Suh, T.-J. Park, W.-I. Kim, I.-K. Hong, J. Power Sources 117 (2003) 1–6.
[14] M. Min, K. Machida, J.H. Jang, K. Naoi, J. Electrochem. Soc. 153 (2006) A334–A338.
[15] J.P. Zheng, P.J. Cygan, T.R. Jow, J. Electrochem. Soc. 142 (1995) 2699–2703.
[16] E. Kolawa, F.C.T. So, W. Flick, X.A. Zhao, E.T. Pan, M.A. Nicolet, Thin Solid Films 173 (1989) 217–224.
[17] I. Zhitomirsky, L. Gal-Or, Mater. Lett. 31 (1997) 155–159.
[18] S. Ardizzone, A. Daghetti, L. Franceschi, S. Trasatti, Colloids Surf. 35 (1989) 85–96.
[19] H.B. Suffredini, V. Tricoli, L.A. Avaca, N. Vatistas, Electrochem. Commun. 6 (2004) 1025–1028.
[20] V. Panic, A. Dekanski, V.B. Miskovic-Stankovic, S. Milonjic, B. Nikolic, J. Electroanal. Chem. 579 (2005) 67–76.
[21] A.E. Gash, T.M. Tillotson, J.H. Satcher Jr., J.F. Poco, L.W. Hrubesh, R.L. Simpson, Chem. Mater. 13 (2001) 999–1007.
[22] A.E. Gash, J.H. Satcher Jr., R.L. Simpson, Chem. Mater. 15 (2003) 3268–3275.
[23] L. Duraes, B.F.O. Costa, J. Vasques, J. Campos, A. Portugal, Mater. Lett. 59 (2005) 859.
[24] J. Livage, M. Henry, C. Sanchez, Prog. Solid State Chem. 18 (1988) 259–341.
[25] B. Dobinson, W. Hofmann, B.P. Stark, The Determination of Epoxides, Pergamon Press, Oxford, 1969.
[26] A.E. Gash, J.H. Satcher Jr., R.L. Simpson, J. Non-Crystal. Solids 350 (2004) 145–151.
[27] T.F. Baumann, A.E. Gash, S.C. Chinn, A.M. Sawvel, R.S. Maxwell, J.H. Satcher Jr., Chem. Mater. 17 (2005) 395–401.
[28] A.E. Gash, T.M. Tillotson, J.H. Satcher Jr., L.W. Hrubesh, R.L. Simpson, J. Non-Cryst. Solids 285 (2001) 22–28.
[29] E.A. Seddon, K.R. Seddon, The Chemistry of Ruthenium, Elsevier, Amsterdam, 1984.
[30] S. Schamm, R. Berjoan, P. Barathieu, Mater. Sci. Eng. B 107 (2004) 58.
[31] D. Briggs, M.P. Seah, Practical Surface Analysis, Wiley, Chicester, 1983, p. 533.
[32] P. Froment, M.J. Genet, M. Devillers, J. Electron Spectrosc. Relat. Phenom. 104 (1999) 119.
[33] D.R. Rolison, P.L. Hagans, K.E. Swider, J.W. Long, Langmuir 15 (1999) 774–779.
[34] L. Ji, J. Lin, H.C. Zeng, Chem. Mater. 13 (2001) 2403–2412.
[35] R. Tannenbaum, C. Hakanson, A.D. Zeno, M. Tirrell, Langmuir 18 (2002) 5592–5599.
[36] P. Mills, J.L. Sullivan, J. Phys. D 16 (1983) 723–732.
[37] J. Pagnaer, D. Nelis, D. Mondelaers, G. Vanhoyland, J. D'Haen, M.K. Van Bael, H. Van den Rul, J. Mullens, L.C. Van Poucke, J. Eur. Ceram. Soc. 24 (2004) 919–923.
[38] P.F. Campbell, M.H. Ortner, C.J. Anderson, Anal. Chem. 33 (1961) 58–61.